

Assessment of the Performance of Inverse Class-F Power Amplifiers in a Discrete Doherty Architecture

*Original*

Assessment of the Performance of Inverse Class-F Power Amplifiers in a Discrete Doherty Architecture / Piacibello, Anna; Zhang, Zhifan; Camarchia, Vittorio. - ELETTRONICO. - (2023), pp. 1-4. ( 2023 International Workshop on Integrated Nonlinear Microwave and Millimetre-Wave Circuits (INMMIC) Aveiro, Portugal 08-11 November 2023) [10.1109/INMMIC57329.2023.10321774].

*Availability:*

This version is available at: 11583/2984273 since: 2023-12-02T16:22:57Z

*Publisher:*

IEEE

*Published*

DOI:10.1109/INMMIC57329.2023.10321774

*Terms of use:*

This article is made available under terms and conditions as specified in the corresponding bibliographic description in the repository

*Publisher copyright*

IEEE postprint/Author's Accepted Manuscript

©2023 IEEE. Personal use of this material is permitted. Permission from IEEE must be obtained for all other uses, in any current or future media, including reprinting/republishing this material for advertising or promotional purposes, creating new collecting works, for resale or lists, or reuse of any copyrighted component of this work in other works.

(Article begins on next page)

# Assessment of the Performance of Inverse Class-F Power Amplifiers in a Discrete Doherty Architecture

Anna Piacibello  
Politecnico di Torino, Italy  
0000-0001-5007-0005

Zhifan Zhang  
Politecnico di Torino, Italy

Vittorio Camarchia  
Politecnico di Torino, Italy  
0000-0002-7294-6773

**Abstract**—This work presents an assessment, at simulation and experimental levels, of the performance of inverse class-F power amplifiers in a Doherty architecture. Two connectorized amplifier modules, designed for standalone operation, are adopted to construct a quasi-balanced Doherty architecture exploiting 3-dB 90° hybrid couplers at the input and output to demonstrate the concept. The Doherty architecture shows competitive performance at 1.8 GHz, with 43 dBm output power and around 60% efficiency from saturation to 6 dB output power back-off. The performance is in line with the state of the art of integrated load-modulated amplifiers, demonstrating the validity of the approach.

**Index Terms**—Continuous mode, Doherty power amplifier, GaN, harmonic tuning, microwave radios

## I. INTRODUCTION

The Doherty power amplifier (DPA) [1] is currently the most widely adopted solution for the design of radio frequency power amplifiers in communication bands below 6 GHz. One of the key aspects of its success is the relative simplicity of the design of its building blocks and the robustness it demonstrates, especially in narrow fractional bandwidths. When aiming for wide bandwidth, specific solutions such as separate inputs for the Main and Auxiliary branches [2], [3] may be required. However, these approaches reduce the advantages of the classical DPA implementation. If simple fully-analog DPA architectures are to be maintained, broadband designs often employ class-AB [4] and class-C stages, low-order matching networks and symmetrical configurations to maintain matching and phase alignment between the two branches over the desired working band [5].

Single-device harmonically tuned PAs can achieve very high efficiency at saturation [6], making them appealing as fundamental components in DPA [7], [8] and Load Modulated Balanced Amplifier (LMBA) [9]–[12] designs, especially since the formulation of continuous modes allows to maintain high efficiency over very wide bands. However, these PAs often require high-order matching networks to synthesise the desired loading conditions at the fundamental and harmonic frequencies. Therefore, incorporating them in a DPA can pose significant challenges if the architecture is not adequately optimized. Moreover, the correct harmonic-generating conditions must be enforced, which is not always possible, especially for class-C devices [13]. It is crucial to carefully optimize all of these design parameters to achieve optimal performance.

In this work, we explore the potential of adopting a continuous mode inverse class-F PA, formerly designed for standalone operation, in a DPA architecture based on a quasi-balanced configuration, utilizing 3-dB 90° hybrid couplers for power splitting at the input and Doherty power combining at the output [14]. This choice allows an implementation based on connectorized components matched to 50  $\Omega$  and serves as a demonstration of the concept. Measurements at 1.8 GHz demonstrate saturated output power of 43 dBm, and efficiency higher than 60% in a 6-dB output power back-off (OBO) range, highlighting the potential of harmonic tuning in DPAs.

## II. DPA OPERATION ANALYSIS AND IMPLEMENTATION

The amplifier used as a building block in the DPA architecture is a continuous inverse class-F amplifier, whose design and characterization are described in detail in [15]. Its Output Matching Network (OMN) is a 5-th order filter, which allows synthesising the targeted high-efficiency loads over the 1.4–2 GHz, thus achieving saturated efficiency higher than 70% over the whole band.

To assemble a DPA using connectorized amplifiers for the Main and Auxiliary stages, it is necessary to implement the combiner on a 50  $\Omega$  impedance and ensure the proper phase relationship between the two branches. Besides, for the Main amplifier, the overall phase rotation from its drain current generator plane to the combiner plane should be a multiple of 180° to maintain the correct load modulation. Since the PA to be used in both branches was not designed specifically to be employed in a DPA configuration, the phase rotation of its OMN may not be optimal. Additionally, the presence of SMA connectors and adapters to connect the various blocks adds further phase delays that should be accounted for.

The phase of  $S_{22}$  of the individual inverse class-F PA, when the active device is off, can be verified to have an overall rotation of around 360° over its operating band, due to the high-order OMN. This has two implications for the implementation of a DPA. Firstly, the Main will not maintain the optimal load modulation over the whole band. Secondly, the Auxiliary amplifier may not present a good open circuit at the output common node at all frequencies before its turn-on point, thus limiting the DPA operating band, if the phase alignment is optimized at center frequency.

After adding an appropriate output offset line ( $\theta_{\text{out}} = 140^\circ$ ) for the overall phase rotation of the OMN to be a multiple

of  $180^\circ$  at center frequency, the load  $R_L$  of the individual PA is modulated from  $50\Omega$  to  $100\Omega$  in simulation and the corresponding loading conditions of the individual PA are observed, to assess its suitability for DPA operation.

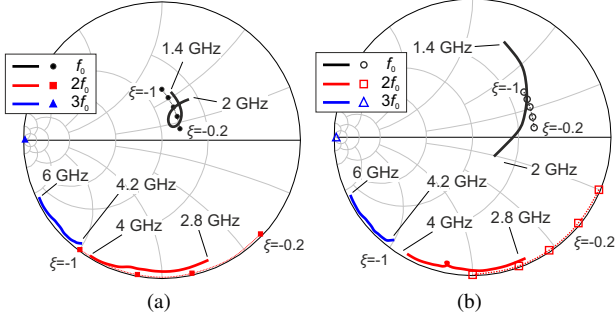


Fig. 1: Target (symbols) and synthesized (solid) load impedances at the current generator plane, (a) at saturation [15] and (b) at 6 dB back-off.

Fig. 1 shows the target loads predicted by theory when  $R_L=50\Omega$ ,  $100\Omega$  and compares them to the loads synthesized by the OMN in the actual PA. As detailed in [15], where these curves are shown only at saturation ( $R_L=50\Omega$ ), the explored continuous mode region corresponds to  $-1 \leq \xi \leq -0.2$ . It can be seen that the target fundamental load trajectories are modulated by a factor of 2, whereas the second harmonic is only slightly rotated counterclockwise and the third is unchanged. As for the synthesized loads at 6-dB OBO, while the harmonic ones are basically unaffected by the modulation of  $R_L$ , the fundamental loads are correctly shifted close to the target around center frequency and deviate from it at the band edges. The most critical deviation is at the upper edge (2 GHz), where the real part of the impedance changes more severely. Overall, the expected output loading conditions suggest that the PA can be successfully employed in a DPA operating around its center frequency (1.75 GHz) and that the resulting architecture is expected to have a narrower bandwidth than the original single-stage PAs.

Two different types of combiners can be used in the DPA architecture, namely the standard quarter-wavelength transformer-based combiner, which is commonly used in DPA designs, or a 3 dB  $90^\circ$  hybrid coupler to implement a quasi-

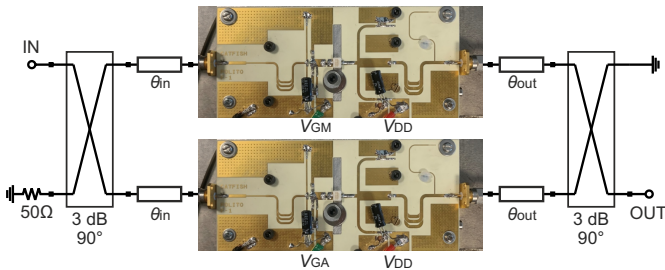


Fig. 2: Block diagram of the discrete DPA architecture.

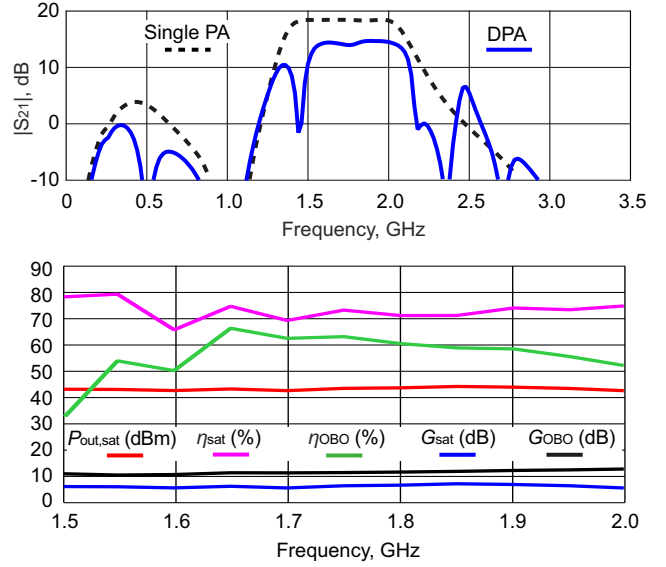


Fig. 3: Simulated optimal performance of the DPA:  $|S_{21}|$  compared to the single PA's (top), and large signal (bottom).

balanced DPA [14]. The latter is chosen as it is more convenient for a discrete-components implementation since it does not require to synthesize and connectorize an *ad-hoc* combiner. As shown in Fig. 2, the architecture is assembled using two connectorized couplers.

If the DPA architecture of Fig. 2 is simulated assuming output phase re-alignment and ideal hybrid couplers (lossless and with infinite bandwidth), it achieves the optimal small and large signal performance shown in Fig. 3. Note that the input

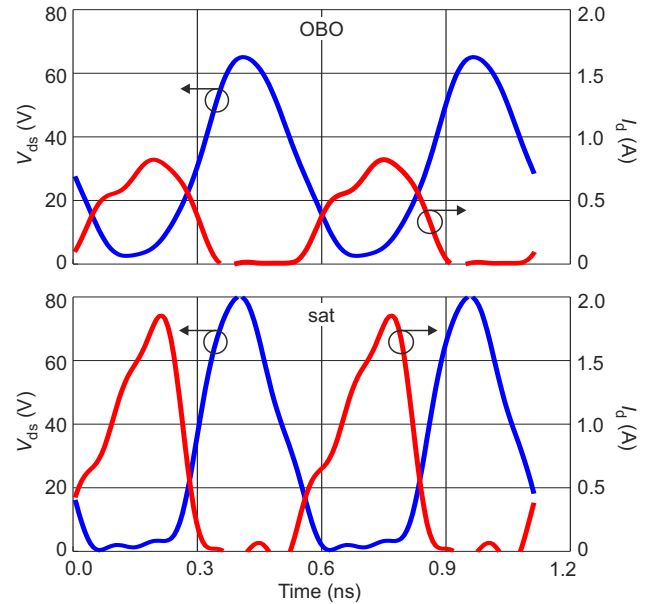


Fig. 4: Simulated drain voltage (blue) and current (red) waveforms at the current generator plane at 1.8 GHz: at 6 dB OBO (top) and at saturation (bottom).

phase alignment  $\theta_{in}$  is immaterial, as long as it is symmetric, apart from the effect of losses on gain and PAE.

Fig. 4 reports the simulated drain waveforms of the Main device at the current generator planes, according to the nonlinear model provided by the transistor manufacturer, at 1.8 GHz, at 6 dB OBO and at saturation. They are fairly in agreement with the ones predicted by theory and simulated in [15], considering that at 6 dB OBO the voltage clipping is not as hard as it is saturation. Also, a  $2 \times$  scaling of the current peak is observed while the waveform shape is reasonably maintained.

### III. DPA ASSEMBLY AND CHARACTERIZATION

The discrete-components DPA architecture has been assembled by connecting two (nominally) identical PA modules to two connectorized  $90^\circ$  hybrids at the input and output. Since narrowband couplers operating around 1.8 GHz were available, the demonstrator was tested at a single frequency.

Ensuring the proper input and output phase alignment, in the case of discrete component assembly, implies carefully estimating the delay introduced by all the adopted SMA launchers, connectors, and adapters. The estimated phase shift at center frequency is  $15^\circ$  for each SMA launcher and around  $20^\circ$  for the available Male-Male and Female-Male adapters. Therefore, considering two launchers and an integer number of adapters, the synthesized  $\theta_{out}$  can be either  $130^\circ$  or  $150^\circ$ , approximately. Due to the limited tuning possibility, the phase cannot be perfectly optimized, thus possibly leading to some performance degradation.

The assembled DPA is characterized under small and large signal Continuous Wave (CW) conditions and the performance is compared to simulations at nominal bias ( $V_{DD}=28$  V,  $V_{GM}=-2.95$  V,  $V_{GA}=-6.5$  V, and  $I_D=60$  mA) and in analogous conditions, i.e., accounting for the sub-optimal phase tuning and real couplers.

Fig. 5 compares the simulated (solid) and measured (symbols) scattering parameters in the range 0.1-3.5 GHz. The agreement is good, with a small signal gain exceeding 10 dB and input and output matching better than -10 dB from 1.6 GHz to 1.9 GHz. The effect of narrowband couplers, as discussed in Section II, is already slightly visible on the small signal bandwidth compared to the estimation of Fig. 3.

The large signal characterization of the prototype DPA was performed using a real-time vector test bench that was calibrated using a 2-port Short-Open-Load-Thru (SOLT) routine. Additionally, an extra calibration step was carried out using a Short-Open-Load (SOL) procedure along with a power meter for absolute power calibration.

The large signal characterization reported in Fig. 6 at 1.8 GHz shows a good agreement between simulations and measurements. The DPA achieves a saturated output power of 43 dBm and maintains a PAE higher than 60% from saturation to 6 dB OBO, thus highlighting the potential of this approach for designing cost-effective DPAs. The achieved performance is very well in line with the estimation of Fig. 3 at the same frequency, apart from a slightly lower saturated efficiency which is due to the losses in the adapters and couplers.

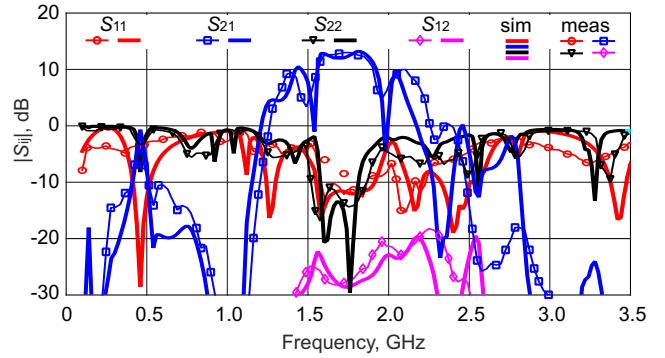


Fig. 5: Comparison between simulated (solid) and measured (symbols) scattering parameters in the range 0.1 GHz–3.5 GHz.

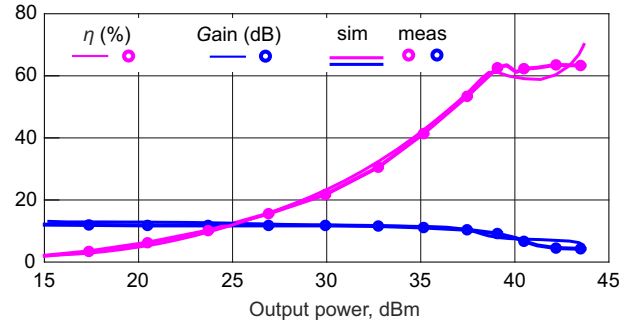


Fig. 6: Comparison between simulated (solid) and measured (symbols) power sweeps at 1.8 GHz.

This suggests that, if wideband couplers were available, the DPA could maintain similar performance on the 1.6-2 GHz band, thus exploiting most of the band of the original PA components. As shown in Table I, the measured performance is also fairly in line with state-of-the-art integrated DPAs and LMBAs at similar frequencies.

TABLE I: Comparison with previously published single-input DPAs and LMBAs.

Ref.	Technique	Freq. (GHz)	$P_{sat}$ (dBm)	$DE_{sat}$ (%)	$DE_{OBO}$ (%)
[7]	DPA	2.14	35	55	50
[8]	DPA	2–2.6	41.7–43.8	61–75	45–64
[5]	DPA	1.8–2.3	43	63–74	50–57
[16]	DPA	2.8–3.6	43–44.2	62–76	44–56
[9]	LMBA	1.8–3.8	44	46–70	33–49
[10]	PD-LMBA	1.5–2.7	42.5	58–72	47–61
[11]	CM-LMBA	1.45–2.45	45.6–46.7	67–78	51–64
[12]	LMBA	2.4	43	54	49
<b>T. W.</b>	<b>DPA</b>	<b>1.8</b>	<b>43</b>	<b>63</b>	<b>60</b>

### IV. CONCLUSION

This paper has presented a quasi-balanced DPA, implemented using two connectorized inverse class-F amplifiers and 3-dB  $90^\circ$  hybrid couplers. The strategy to properly assemble the architecture is discussed and a discrete-components

prototype is fabricated and measured. It exhibits promising performance at center frequency, validating its suitability for communications applications. These results demonstrate the possibility to enhance the back-off efficiency thanks to harmonic tuning and validate its feasibility even in a discrete implementation that adopts connectorized components. By integrating wideband couplers and carefully tuning the offset lines, it is possible to address the bandwidth limitation, enabling the DPA to operate efficiently across a wider bandwidth.

#### ACKNOWLEDGEMENT

This research was supported by the Project Programma Operativo Nazionale (PON) Ricerca e Innovazione “Tecnologie abilitanti e architetture innovative per future generazioni (6G) di trasmettitori intelligenti green” (DM 1062/21, CUP E15F21003760001) funded by the Italian Ministry of University and Research (MUR).

#### REFERENCES

- [1] V. Camarchia *et al.*, “The Doherty power amplifier: Review of recent solutions and trends,” *IEEE Trans. Microw. Theory Techn.*, vol. 63, no. 2, pp. 559–571, Feb. 2015.
- [2] A. Piacibello *et al.*, “Dual-input driving strategies for performance enhancement of a Doherty power amplifier,” in *2018 IEEE MTT-S International Wireless Symposium (IWS)*, 2018, pp. 1–4.
- [3] —, “Comparison of S-band Analog and Dual-Input Digital Doherty Power Amplifiers,” in *2018 13th European Microwave Integrated Circuits Conference (EuMIC)*, 2018, pp. 269–272.
- [4] M. Iqbal and A. Piacibello, “A 5 W class-AB power amplifier based on a GaN HEMT for LTE communication band,” in *2016 16th Mediterranean Microwave Symposium (MMS)*, 2016, pp. 1–4.
- [5] M. Yang, J. Xia, and A. Zhu, “A 1.8–2.3 GHz broadband Doherty power amplifier with a minimized impedance transformation ratio,” in *2015 Asia-Pacific Microwave Conference (APMC)*, vol. 1, 2015, pp. 1–3.
- [6] M. Iqbal and A. Piacibello, “GaN HEMT based class-F power amplifier with broad bandwidth and high efficiency,” in *2016 International Conference on Integrated Circuits and Microsystems (ICICM)*, 2016, pp. 131–134.
- [7] P. Colantonio, F. Giannini, R. Giofre, and L. Piazzon, “Efficiency improvement in Doherty power amplifier by using Class F approach,” in *2009 European Microwave Integrated Circuits Conference (EuMIC)*, 2009, pp. 17–20.
- [8] F. Meng, Y. Sun, L. Tian, and X.-W. Zhu, “A broadband high-efficiency Doherty power amplifier with continuous inverse class-F design,” in *2017 XXXIInd General Assembly and Scientific Symposium of the International Union of Radio Science (URSI GASS)*, 2017, pp. 1–3.
- [9] P. H. Pednekar, E. Berry, and T. W. Barton, “RF-Input Load Modulated Balanced Amplifier With Octave Bandwidth,” *IEEE Trans. Microw. Theory Techn.*, vol. 65, no. 12, pp. 5181–5191, 2017.
- [10] Y. Cao and K. Chen, “Pseudo-Doherty Load-Modulated Balanced Amplifier With Wide Bandwidth and Extended Power Back-Off Range,” *IEEE Trans. Microw. Theory Techn.*, vol. 68, no. 7, pp. 3172–3183, 2020.
- [11] J. Pang, C. Chu, Y. Li, and A. Zhu, “Broadband RF-Input Continuous-Mode Load-Modulated Balanced Power Amplifier With Input Phase Adjustment,” *IEEE Trans. Microw. Theory Techn.*, vol. 68, no. 10, pp. 4466–4478, 2020.
- [12] K. Vivien *et al.*, “Load Modulated Balanced Amplifier Designed for AM-PM Linearity,” in *2020 50th European Microwave Conference (EuMC)*, 2021, pp. 304–307.
- [13] P. Colantonio, F. Giannini, G. Leuzzi, and E. Limiti, “On the class-F power amplifier design,” *International Journal of RF and Microwave Computer-Aided Engineering*, vol. 9, no. 2, pp. 129–149, 1999.
- [14] H. Lyu, Y. Cao, and K. Chen, “Linearity-Enhanced Quasi-Balanced Doherty Power Amplifier With Mismatch Resilience Through Series/Parallel Reconfiguration for Massive MIMO,” *IEEE Trans. Microw. Theory Techn.*, vol. 69, no. 4, pp. 2319–2335, 2021.
- [15] A. Piacibello, Z. Zhang, and V. Camarchia, “Continuous Inverse Class-F GaN Power Amplifier with 70% Efficiency over 1.4-2 GHz Bandwidth,” in *2023 IEEE Topical Conference on RF/Microwave Power Amplifiers for Radio and Wireless Applications*, 2023, pp. 10–12.
- [16] A. Nasri *et al.*, “Design of a Wideband Doherty Power Amplifier with High Efficiency for 5G Application,” *Electronics*, vol. 10, no. 8, 2021. [Online]. Available: <https://www.mdpi.com/2079-9292/10/8/873>